ELECTRONIC SUPPLEMENTARY INFORMATION

Atom Transfer between Precision Nanoclusters and Polydispersed Nanoparticles: A Facile Route for Monodispersed Alloy Nanoparticles and their Superstructures

Paulami Bose,[a] Papri Chakraborty,‡[a] Jyoti Sarita Mohanty,‡[a] Nonappa,[b] Angshuman Ray Chowdhuri,[a] Esma Khatun,[a] Tripti Ahuja,[a] Ananthu Mahendranath,[a,c] and Thalappil Pradeep*[a]

[a]DST Unit of Nanoscience (DST UNS) and Thematic Unit of Excellence (TUE), Department of Chemistry, Indian Institute of Technology Madras, Chennai 600 036, India.

[b] Faculty of Engineering and Natural Sciences, Tampere University, P.O. Box 541, FI-33101 Tampere, Finland.

[c]Department of Metallurgical and Materials Engineering, Indian Institute of Technology Madras, Chennai 600036, India.

*E-mail: pradeep@iitm.ac.in

‡ Authors contributed equally.

TABLE OF CONTENT

Instrumentation

UV-Vis Spectroscopy: Perkin Elmer Lambda 25 instrument was used for optical absorption spectra recording having a range of 200 – 1100 nm with a band pass filter of 1 nm.

HRTEM: High-resolution transmission electron microscopy (HRTEM) imaging was carried out on a JEOL 3010, 300 kV instrument with a UHR polepiece. Energy dispersive analysis (EDS) was performed using an Oxford EDAX connected to the HRTEM. A Gatan 794 multiscan CCD camera was used to capture the images. Samples were prepared by dropcasting the dispersion on carbon coated copper grids (spi Supplies, 3530C-MB) and dried at ambient conditions.

MALDI MS: Matrix Assisted Laser Desorption Ionization Mass Spectrometer (MALDI MS) data were collected using Voyager-DE PRO Biospectrometry Workstation from Applied Biosystems.

A solution in 0.5 mL of dichloromethane (DCM) was made with about 6.2 mg of Trans-2-[3-(4-tertbutylphenyl)-2-methyl-2- propenylidene]malononitrile (DCTB, > 98%) matrix and it

was used for the MALDI MS measurements. Roughly 1 part of sample dissolved in DCM and 2 parts of the prepared DCTB matrix solution were mixed thoroughly and spotted on the sample plate and was left to dry at ambient conditions. In order to minimize fragmentation of the sample, all the measurements were carried out at the laser fluence. Desorption and ionization was carried out with a 337 nm Nitrogen laser. Mass spectra were recorded in linear positive ion and/or negative ion mode and were averaged for nearly 250 shots. Accelerating voltage was kept at 20 kV.

ESI MS: All the mass spectrometric measurements were carried out in a Waters SYNAPT G2-Si instrument. The instrument is well equipped with electrospray ionization, and all spectra were measured in the negative ion and resolution mode. The instrument has the capability of measuring ESI MS with high-resolution up to the orders of 50,000 (m/Dm). NaI was used for calibrating the instrument. The measurement conditions were optimized to a capillary voltage of 3 kV, a cone voltage of 20 V, a desolvation gas flow of 400 liters/hour, a source temperature of 100°C, a desolvation temperature of 150°C, and a sample infusion rate of 30 ml/hour.

All the mass spectrometric measurements were done in a Waters SYNAPT G2-Si instrument. The instrument is well equipped with ESI, and all spectra were measured in the negative ion and resolution mode. The instrument is capable of measuring ESI MS with high-resolution touching orders of 50,000 (m/Dm). The instrument was calibrated using NaI. An optimized condition involving a capillary voltage of 3 kV, a cone voltage of 20 V, a desolvation gas flow of 400 liters/hour, a source temperature of 100°C, a desolvation temperature of 150°C, and a sample infusion rate of 30 ml/hour was used for all measurements.

Raman Spectroscopy: Raman measurements were carried out using a WITec GmbH alpha300S confocal Raman equipped with a 532 nm laser as the excitation source. Measurements involved a 20× objective (Plan-Apochromat, Zeiss), 600 grooves/mm grating for 1 s acquisition time. A laser power of ~800 µW was maintained on the sample throughout the measurement.

Serial EM and Electron Tomography Reconstruction: The transmission electron microscopy (TEM) images were collected using JEM 3200FSC field emission microscope (JEOL) operated at 300 kV in bright field mode with Omega-type Zero-loss energy filter. The images were

acquired with Gatan digital micrograph software while the specimen temperature was maintained at -187°C. For transmission electron tomographic reconstruction, tilt series of 2D projections were acquired with the SerialEM-software package.[1,2] Specimen was tilted between ±69° angles with 2-3° increment steps under low dose mode.[3] The acquired raw stack of images was first subjected for a series of pre-processing, coarse alignment, final alignment and further aligned using IMOD software package.[4] The final aligned file was then utilized for 3D reconstruction with custom made maximum entropy method (MEM) program with a regularization parameter value of $\lambda = 1.0\ e^{-3}$ on MacPro.[5,6] The 3D isosurface and solid colored images were produced using UCSF Chimera.

Scanning Transmission Electron Microscopy and EDS mapping: The STEM imaging was performed using JEOL JEM-2800 high throughput electron microscope equipped with Schottky type field emission gun operated at 200 kV with simultaneous bright field (BF) and dark field (DF) STEM imaging. For elemental mapping energy dispersive X-ray mapping and spectra were collected using dual silicon drift detectors.

Concentration calculation* for 4 nm Ag@PET nanoparticles case (Fig. 1 A)

Average size of Ag NP (HRTEM), 2R = 4.37 nm

Volume of 1 Ag NP (sphere), $V = \frac{4}{3}\pi R^3 = 43.69\ nm^3$

Density of Ag NPs, $\rho = 10.5\ \frac{g}{cm^3} = 1.05\ \frac{mg}{nm^3}$

Mass of 1 Ag NPs, $m = V\rho = 4.58 \times 10^{-16}$ mg

Weight of Ag NPs (dry weight of the sample), $W = 7.5\ \frac{mg}{3\ mL} = 2.5\ \frac{mg}{L}$

Number of NPs in the sample, $N = \frac{W}{m} = 5.45 \times 10^{18}\ \frac{\text{particles}}{\text{L}}$

Particle molarity of Ag@PET NPs $= \frac{N}{N_A} = 9.05\ \mu M$

Concentration calculation* for 1.8 nm $Au_{25}(PET)_{18}$ nanocluster

Average size of gold nanocluster (HRTEM), 2R = 1.8 nm

Volume of 1 gold nanocluster (sphere), $V = \frac{4}{3}\pi R^3 = 3.05\ nm^3$

Density of gold nanoparticles, $\rho = 19.32\ \frac{g}{cm^3} = 1.93 \times 10^{-17}\ \frac{mg}{nm^3}$

Mass of 1 gold nanocluster, $m = V\rho = 5.89 \times 10^{-17}$ mg

Weight of gold nanocluster (dry weight of the sample), W = 0.9 $\frac{\text{mg}}{0.3\ \text{mL}}$ = 3000 $\frac{\text{mg}}{\text{L}}$

Number of particles in the sample, N = $\frac{W}{m}$ = 5.08 x 10^{19} $\frac{\text{particles}}{\text{L}}$

Particle molarity of gold nanocluster = $\frac{\text{N}}{\text{N}_\text{A}}$ = 84.4 µM

Using, $M_1V_1 = M_2V_2$

Particle molarity (M_2) when 0.3 mL cluster diluted in 3.3 mL DCM = 7.67 µM

Weight of gold nanocluster (dry weight of the sample), W = 8.1 $\frac{\text{mg}}{3\ \text{mL}}$ = 2700 $\frac{\text{mg}}{\text{L}}$

Number of particles in the sample, N = $\frac{W}{m}$ = 4.57 x 10^{19} $\frac{\text{particles}}{\text{L}}$

Particle molarity of gold nanocluster = $\frac{\text{N}}{\text{N}_\text{A}}$ = 75.99 µM

* For simplicity of calculation, the concentration was calculated in terms of the metal present.

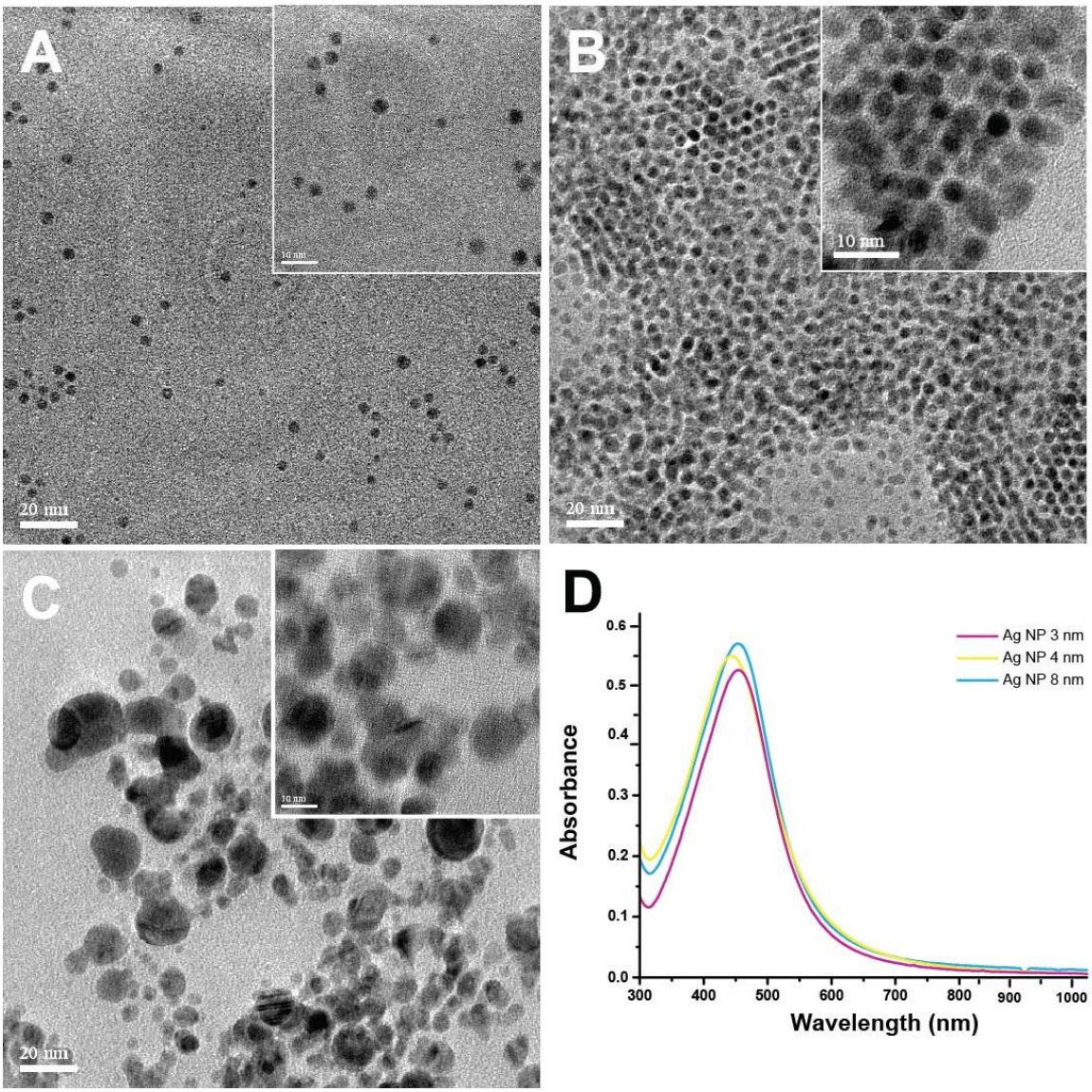

Fig. S1 HRTEM micrographs of Ag@PET NPs of sizes, (A) 3 nm, (B) 4 nm, (C) polydispersed 8 nm, and (D) the corresponding UV-Vis spectra. The mentioned size indicates the most probable diameter of the metallic core of the particle.

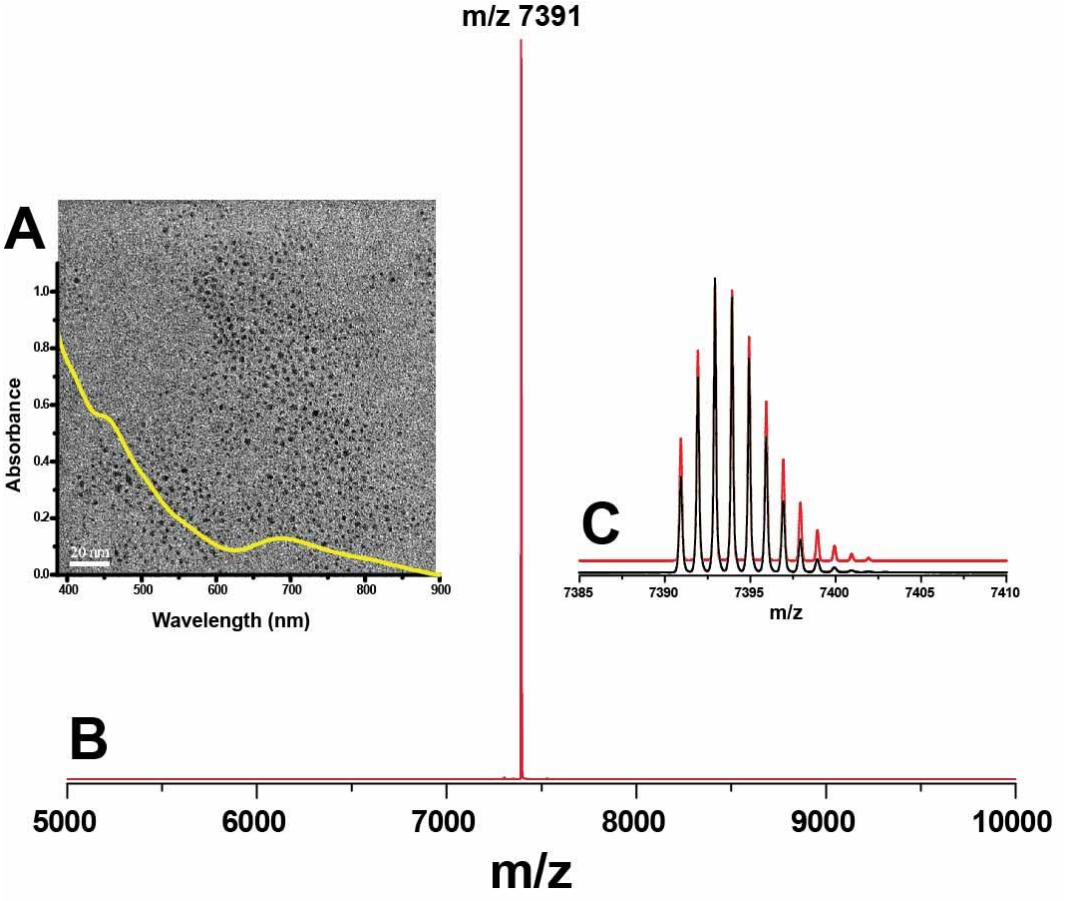

Fig. S2 Characterization of $Au_{25}(PET)_{18}$ NC, (A) HRTEM micrograph and (inset) UV-Vis spectra with characteristic peaks at 397, 445, 552, 683, and 796 nm, (B) ESI MS spectrum of $[Au_{25}(PET)_{18}]^{-}$ NC having a molecular peak at m/z 7391, (C) Experimental (black), and calculated (red) matching for high resolution isotopic distribution of the molecular ion peak. This is in agreement with already reported ESI MS spectra of $Au_{25}(PET)_{18}$ NC.[7,8]

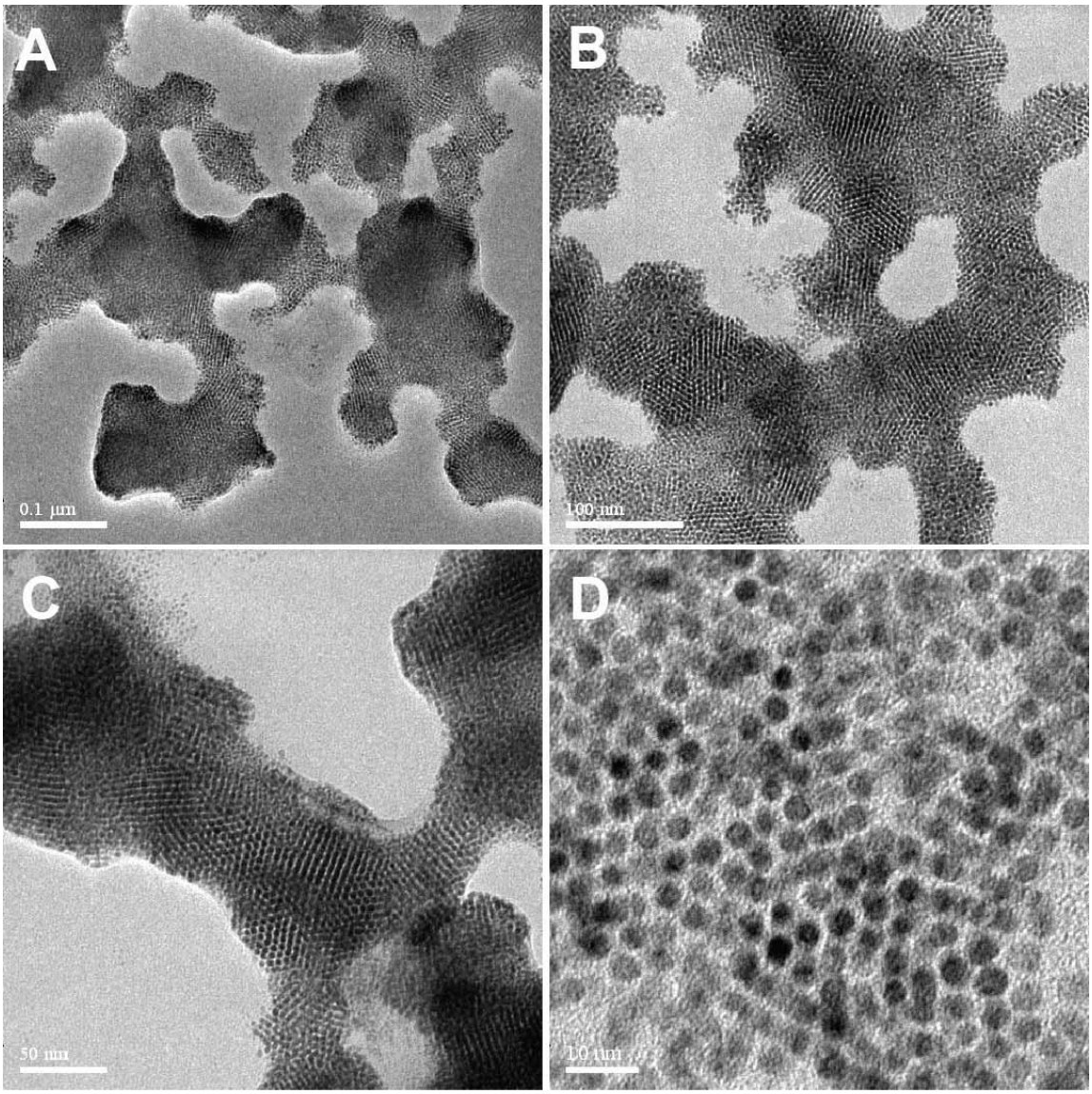

Fig. S3 HRTEM micrographs of the spontaneous assembly formed after the reaction of 4 nm Ag@PET NPs captured at different magnifications, (A) 0.1 µm, (B) 100 nm, (C) 50 nm, and (D) 10 nm. The NPs resulted in the reaction are approximately 3.45 nm.

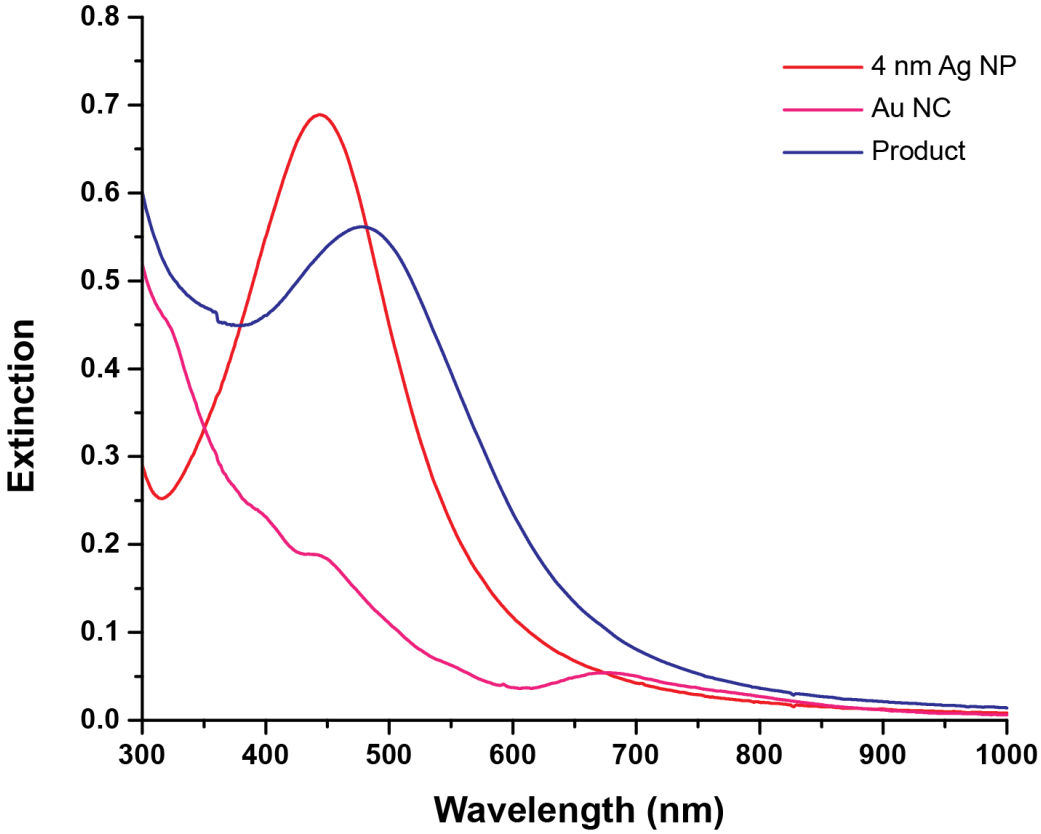

Fig. S4 UV-Vis spectra of 4 nm Ag@PET NPs (red trace), $Au_{25}(PET)_{18}$ NC (magenta trace), and the reaction product (blue trace). The corresponding HRTEM micrographs from the same reaction mixture are already discussed in Fig. 1.

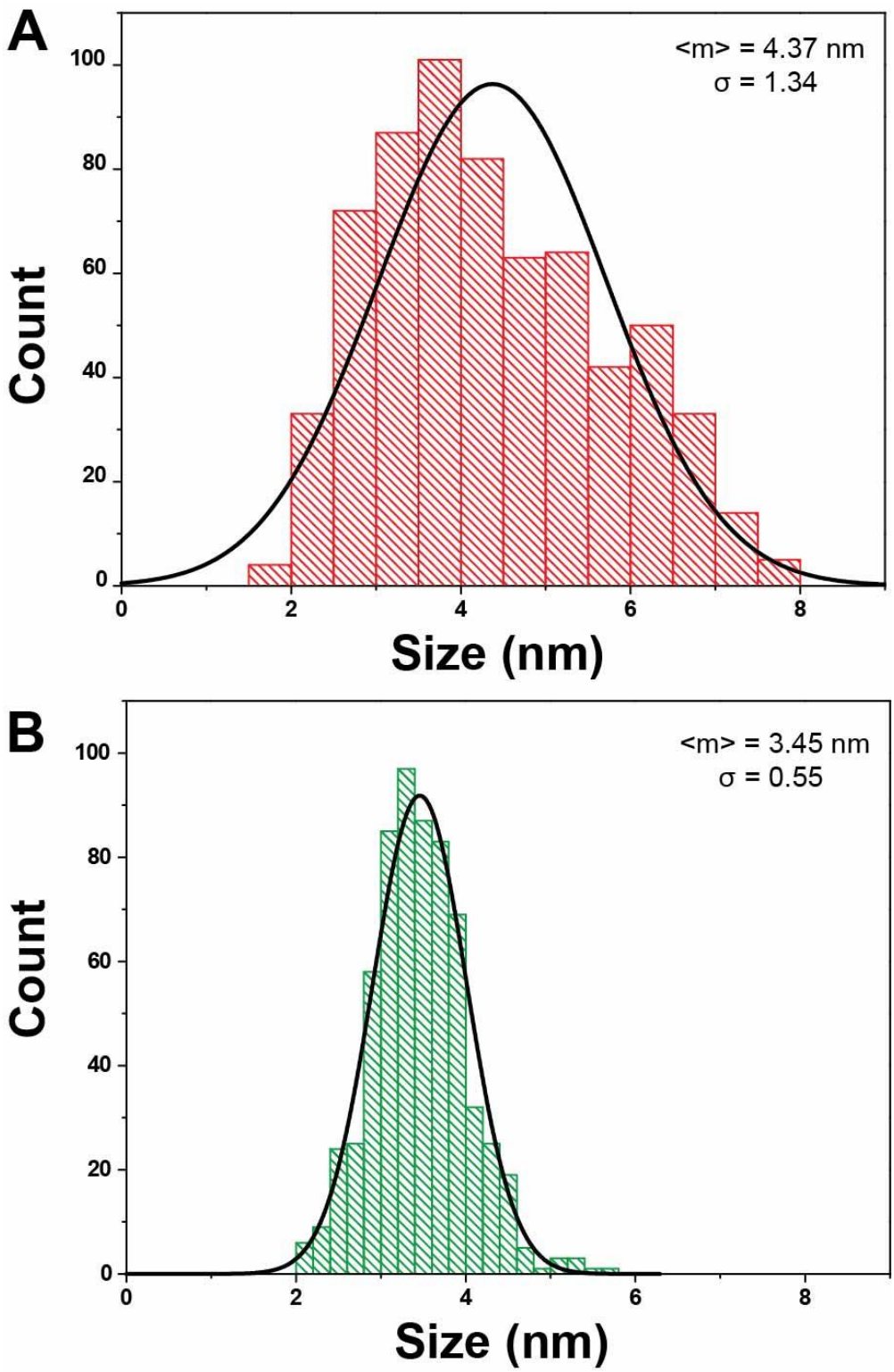

Fig. S5 Particle size distribution of the 4 nm Ag@PET NP reaction case for the (A) parent NPs was 4.37 ± 2.3 nm, and (B) reacted NPs was 3.45 ± 1.2 nm, where <m> and σ are the notations used for mean size and standard deviation, respectively.

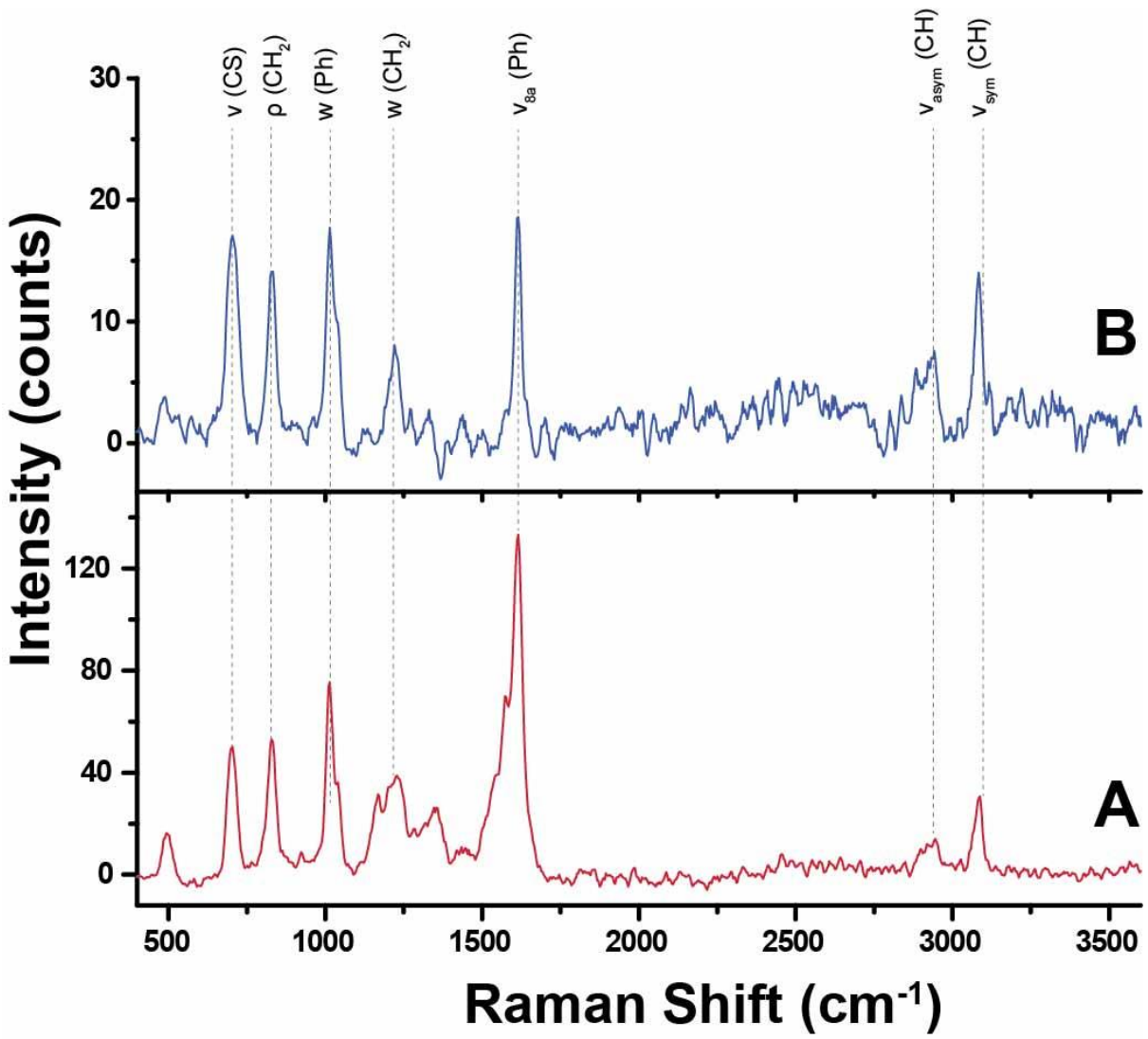

Fig. S6 Raman Spectroscopic analysis of 4 nm Ag@PET NPs (A) before reaction, and (B) after reaction with $Au_{25}(PET)_{18}$ NC (reaction mixture was centrifuged followed by washing with DCM). Here, only the capping agent (2-PET) is Raman active.

Spectral analysis of 2-PET: 699 cm^{-1} (CS symmetric stretch due to *trans* conformation of 2-PET), 823 cm^{-1} (CH_2 rocking), 1005 cm^{-1} (In plane vibration of phenyl ring), 1209 cm^{-1} (CH2 wag), 1600 cm^{-1} (8a In a plane vibration of phenyl ring), 2944 cm^{-1} (CH asymmetric stretch), and 3071 cm^{-1} (CH symmetric stretch)

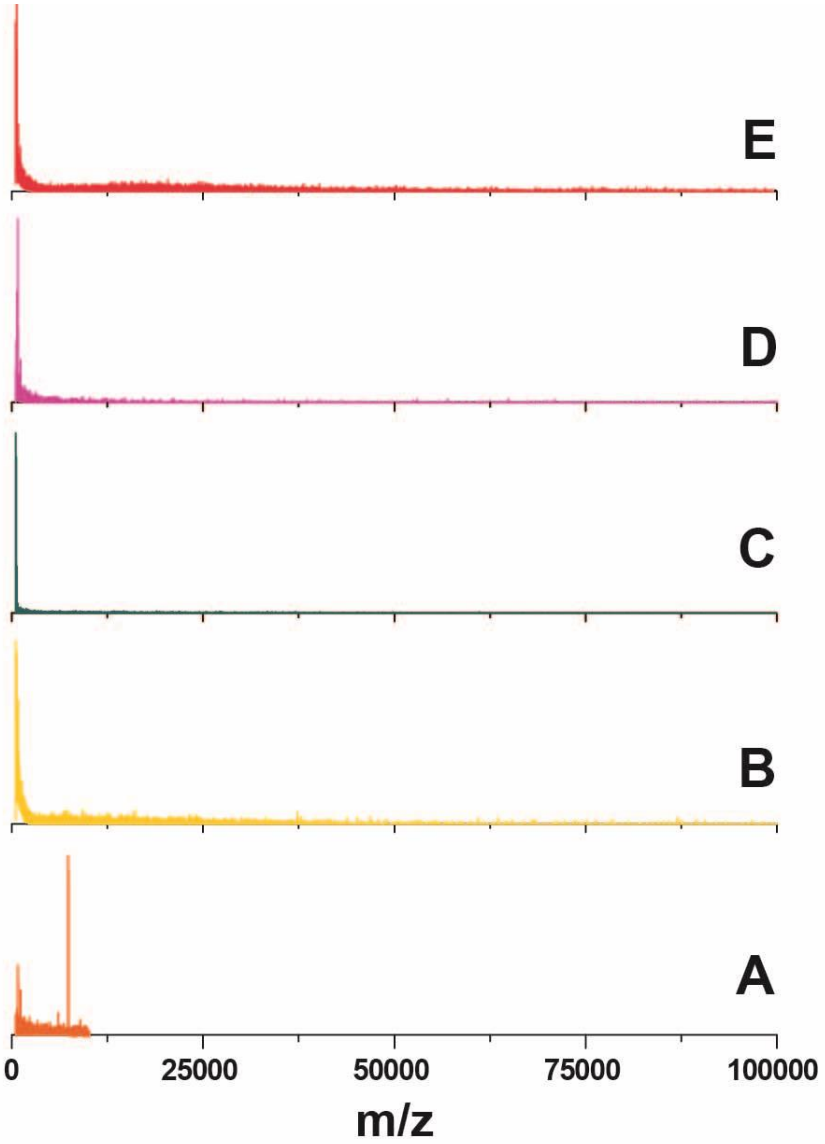

Fig. S7 MALDI MS spectral analysis of the reactants, including, (A) $Au_{25}(PET)_{18}$ NC giving a molecular peak at m/z 7407 in the negative ion mode, 4 nm Ag@PET NPs measured in (B) negative ion mode, and (C) positive ion mode. In case of the Ag NPs, in both the modes signals were absent. Then, the reactants were mixed and allowed to react for 15 min, following which the reaction mixture was subjected to centrifugation and the MALDI MS spectra was collected for both (D) supernatant, and (E) precipitate in the negative ion mode. The absence of peak at m/z 7407 indicates the complete consumption of $Au_{25}(PET)_{18}$ NC during the reaction resulting in the alloy NPs.

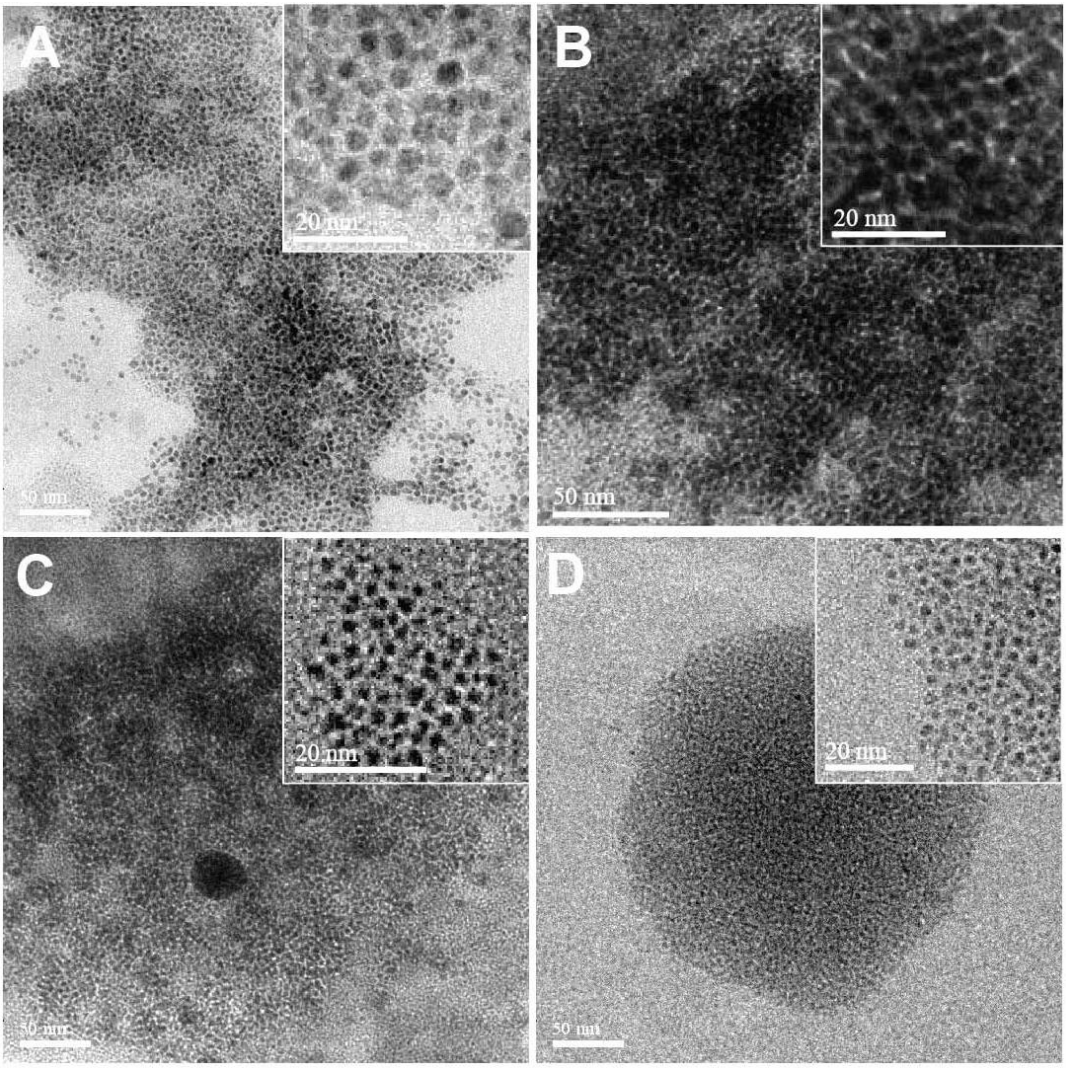

Fig. S8 HRTEM micrographs of the precipitate collected on centrifugation after 15 min from the reaction mixture used for carrying out the ESI MS measurements. Precipitate images on the reaction with (A, B) 4 nm Ag@PET NPs, and (C, D) polydispersed 8 nm Ag@PET NPs. In both the cases, the precipitate HRTEM micrographs are similar to our initial findings in Fig. 1 A, and 3 D.

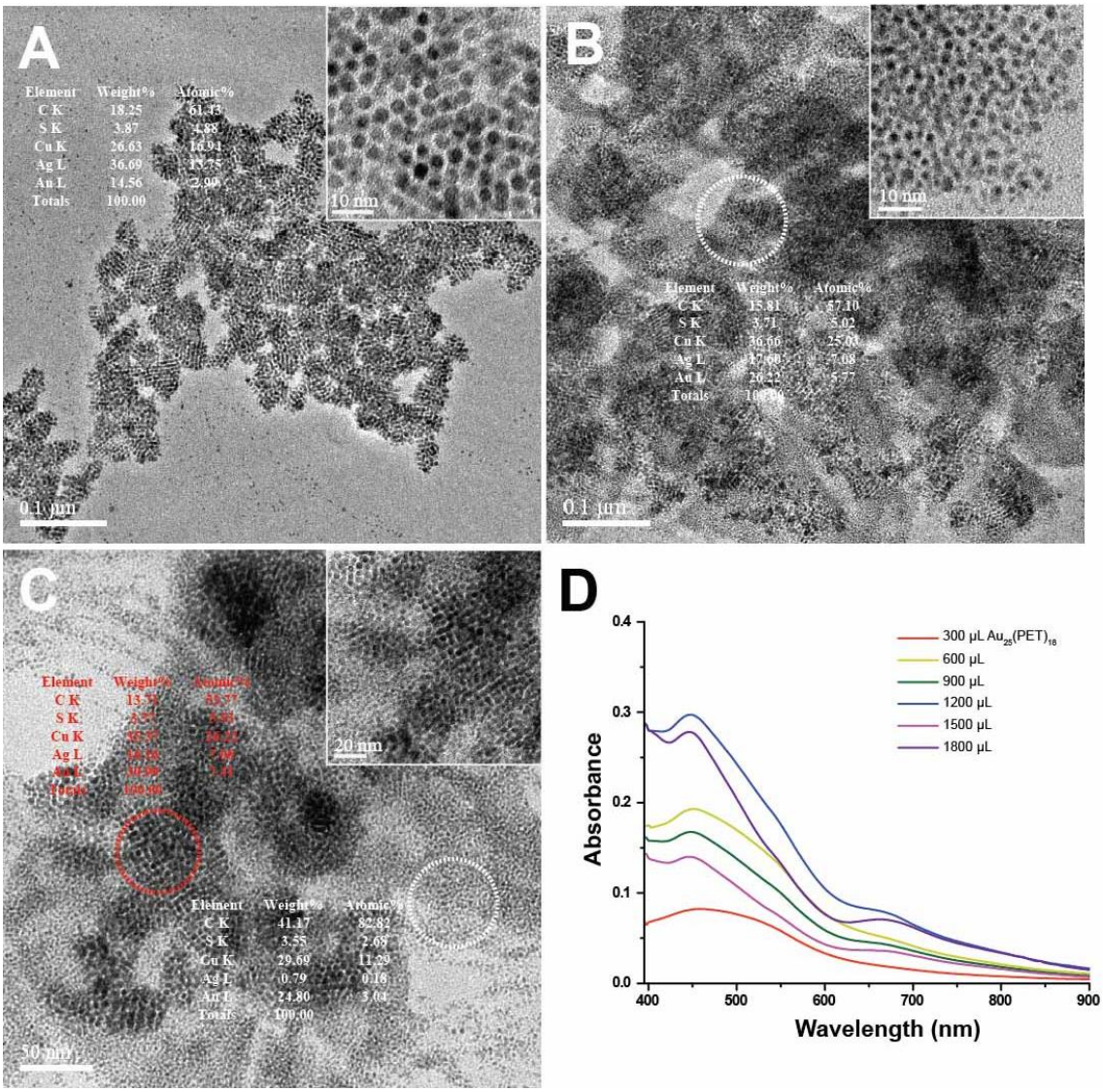

Fig. S9 The concentration dependence of $Au_{25}(PET)_{18}$ NC in the reaction was studied using HRTEM and UV-Vis spectroscopy. The reaction mixture was monitored after adding each 300 µL of $Au_{25}(PET)_{18}$ NC, HRTEM micrographs corresponding to the total cluster added to the reaction mixture, like, (A) 300 µL, (B) 600 µL, and (C) 900 µL. (D) UV-Vis spectra showing the $Au_{25}(PET)_{18}$ NC features getting dominant as the amount of the cluster increases in the reaction medium. Concentrations mentioned in the experimental section.

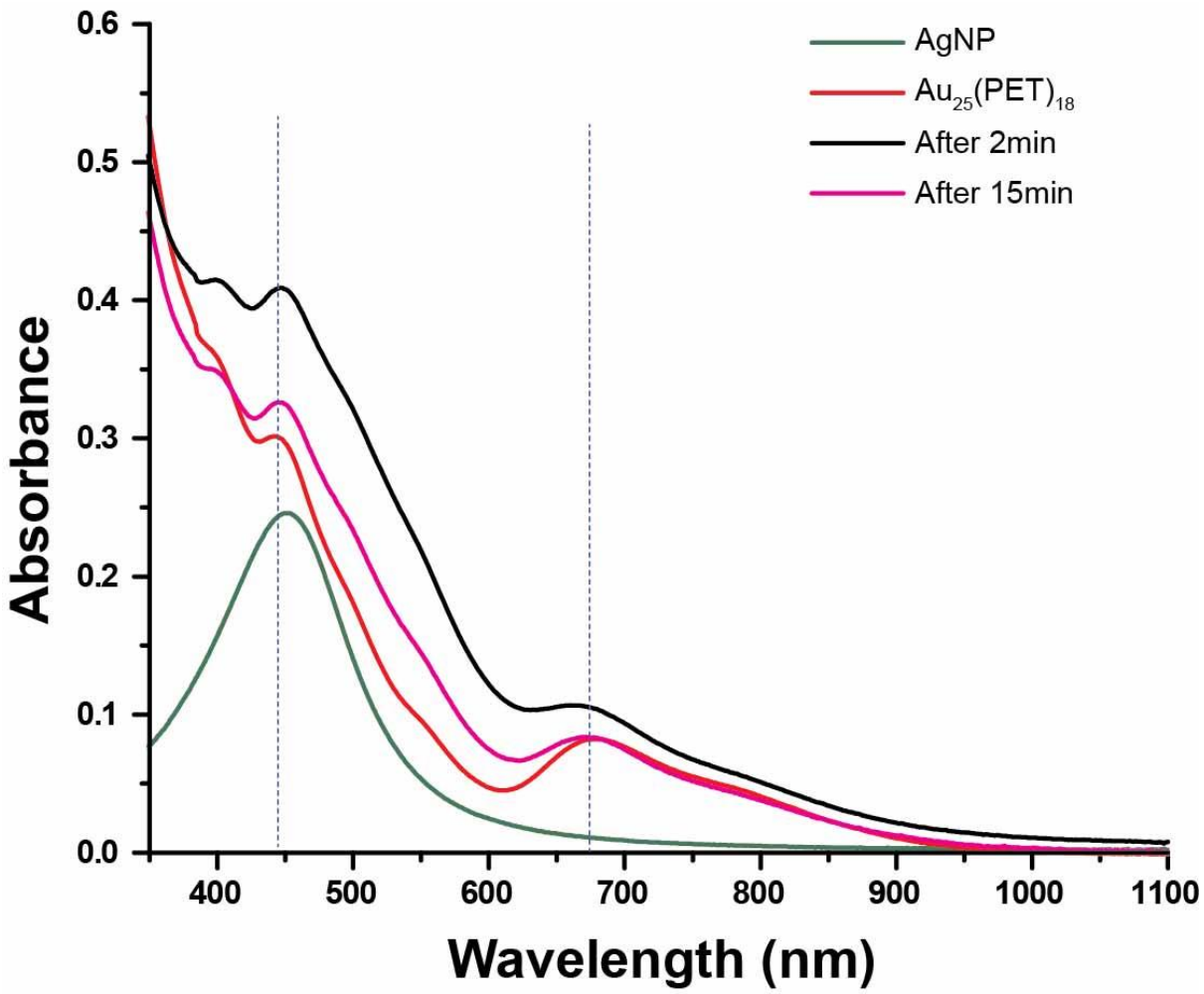

Fig. S10 Kinetic study of the reaction of 4 nm Ag@PET NPs using UV-Vis spectroscopy, Ag@PET NPs (olive trace), $Au_{25}(PET)_{18}$ (red trace), reaction mixture after 2 min (black trace) and 15 min (magenta trace). The blue shift (blue dotted lines) was observed after 2 min (black trace) and after 15 min the spectrum goes back to the original cluster (red trace) like feature. The shift in the UV-Vis spectrum at the 2 min interval suggests generation of new species in the reaction mixture.

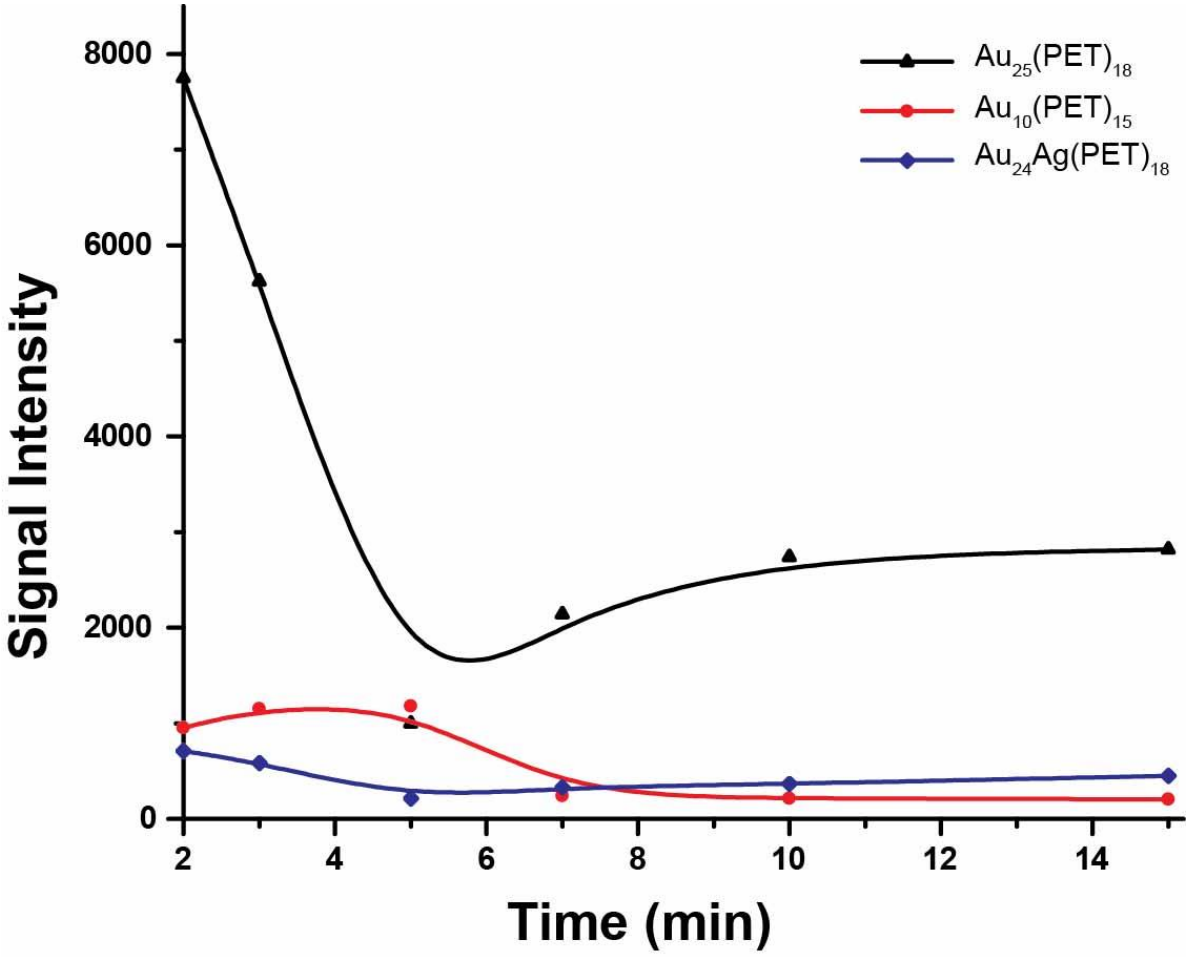

Fig. S11 The evolution of the intermediate species $Au_{24}Ag(PET)_{18}$ and $Au_{10}(PET)_{15}$ can be observed in comparison to the parent $Au_{25}(PET)_{18}$ NC from the plot of signal intensities versus time.

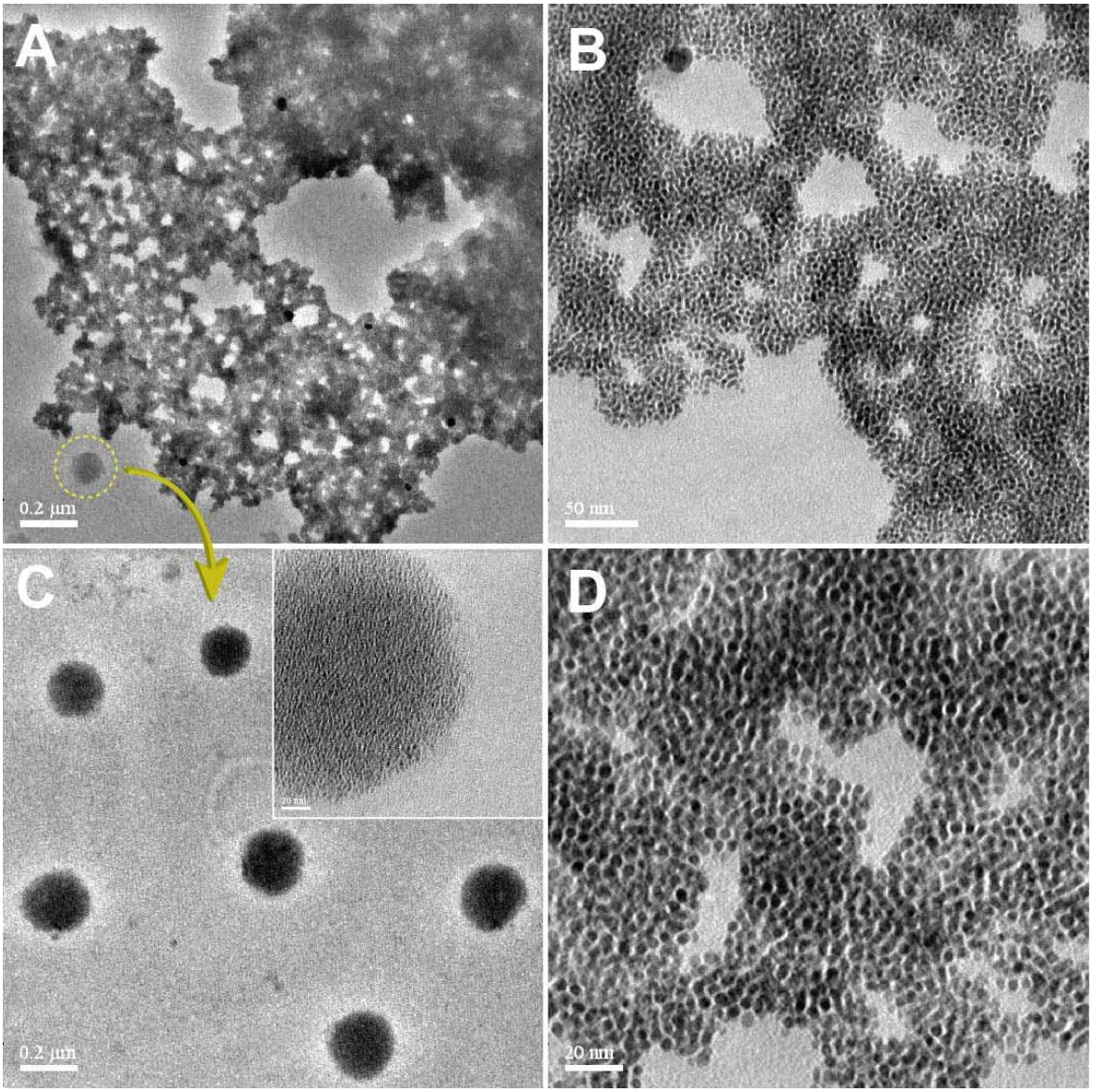

Fig. S12 HRTEM micrographs of the spontaneous assembly formed after the reaction of 8 nm Ag@PET NPs captured at different magnifications, (A) 0.2 µm, it comprises of two kinds of assemblies which further captured at (B) 50 nm, and (C) 0.2 µm (yellow, inset) (D) 20 nm. The NPs resulted in the reaction are approximately 3.73 and 2 nm.

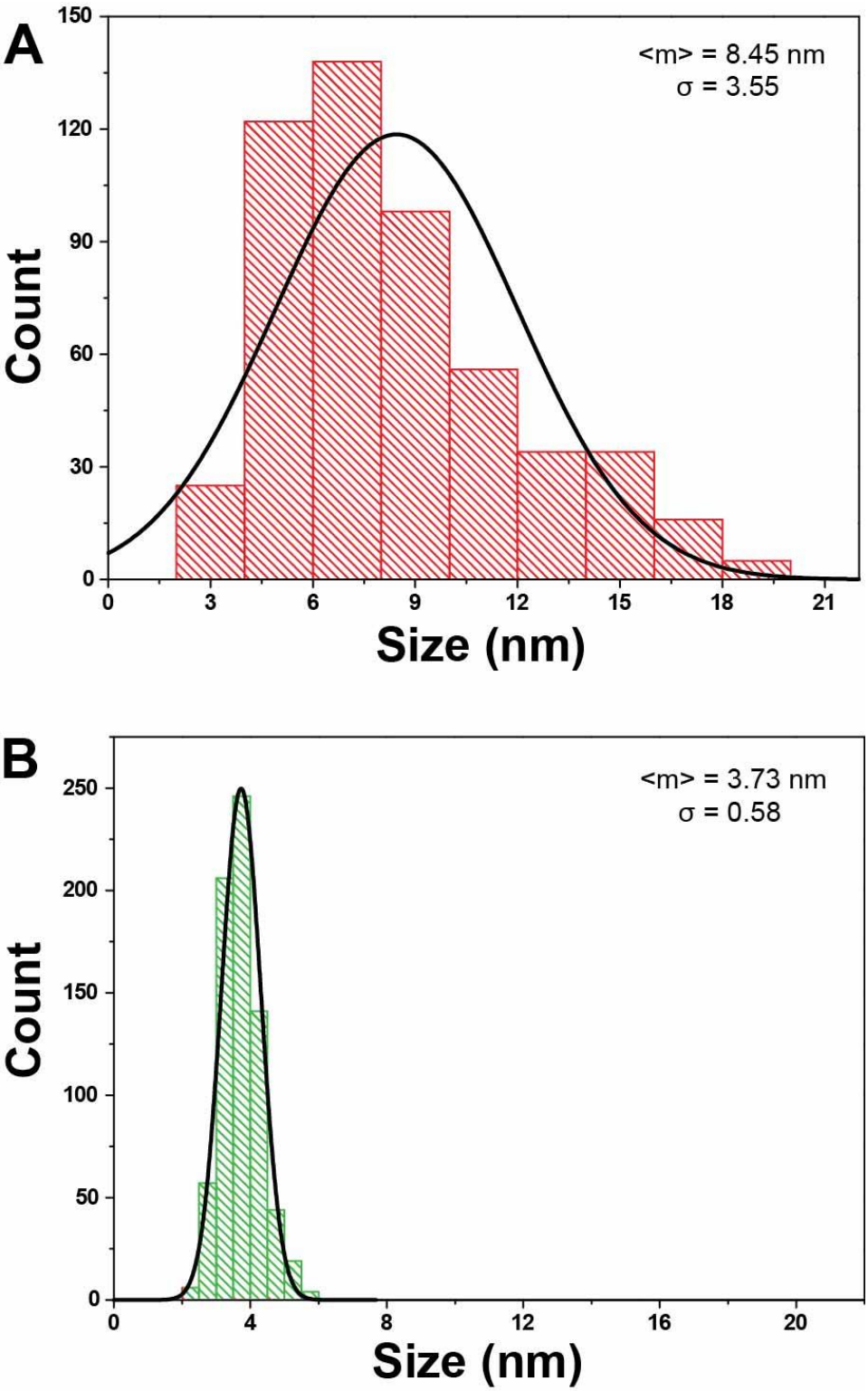

Fig. S13 Particle size distribution of the polydispersed 8 nm reaction case for the (A) parent NPs was 8.45 ± 6.3 nm, and (B) reacted NPs was 3.73 ± 1.0 nm, where <m> and σ are the notations used for mean size and standard deviation, respectively.

Print:12/21/2019 9:18:07 PM Untitled

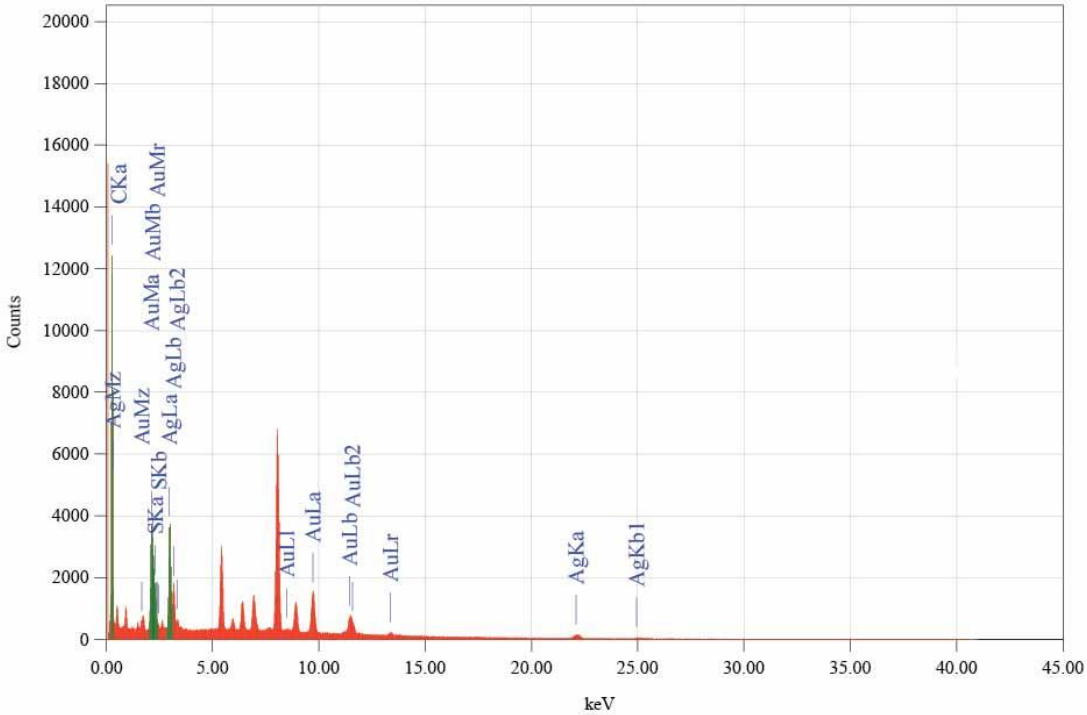

File: Untitled
Specimen ID:
Date: 12/21/2019 9:03:00 PM

Acquisition Parameter

Acc. Voltage	: 200.0 kV	Probe Current	: 1.00000 nA
Real Time	: 539.20 sec	Dead Time	: 2 %
Live Time	: 524.26 sec	Counting Rate	: 1654 Counts/sec
Preset	: Off		
Energy Range	: 0 - 40 keV	PHA Mode	: T3

Thin Film Standardless Standardless Quantitative Analysis
Fitting Coefficient : 0.6465

Element	(keV)	Mass%	Counts	Sigma	Atom%	Compound	Mass%	Cation	K
H *									
C K* (Ref.)	0.277	48.24	80092.55	0.16	88.76				1.0000
S K !	2.307	5.11	14664.02	0.09	3.52				0.5790
Ag L	2.984	26.78	51228.97	0.19	5.49				0.8679
Au M	2.120	19.86	36503.52	0.19	2.23				0.9032
Total		100.00			100.00				

Fig. S14 Spot EDS spectrum of the reacted particle (Fig. 4A). Elemental composition was quantified for the presence of Sulfur (S), Silver (Ag), and Gold (Au) present in the superlattice.

Print:12/23/2019 4:09:41 PM Untitled

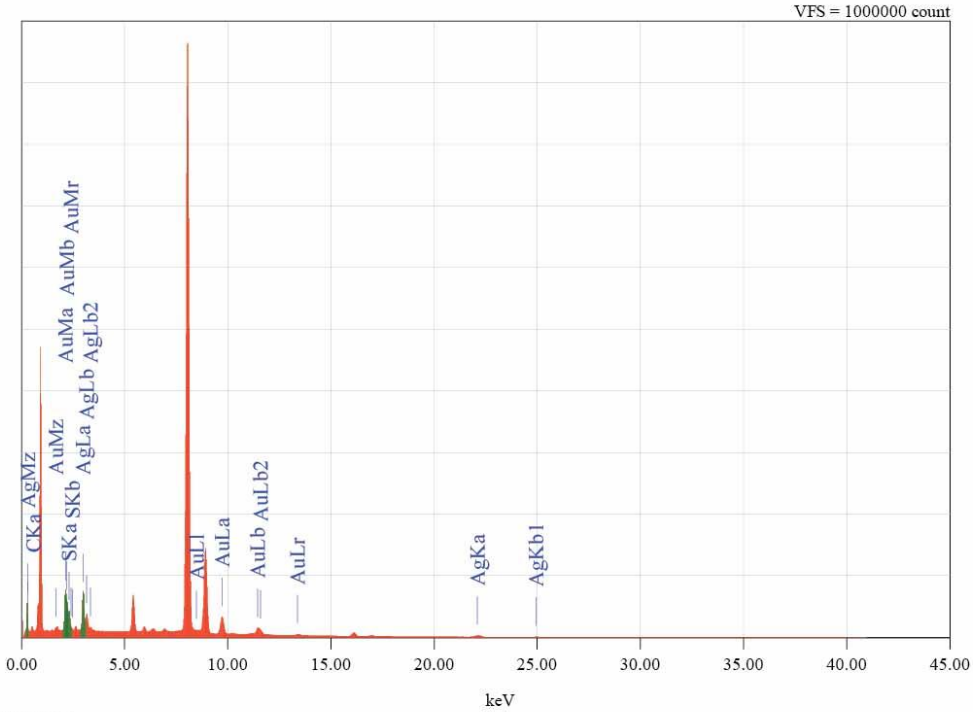

File: Untitled
Specimen ID:
Date: 12/23/2019 3:25:44 PM

Acquisition Parameter

Acc. Voltage	:	200.0 kV	Probe Current	:	1.00000 nA
Real Time	:	2125.89 sec	Dead Time	:	64 %
Live Time	:	524.11 sec	Counting Rate	:	102273 Counts/sec
Preset	:	Off			
Energy Range	:	0 - 40 keV	PHA Mode	:	T3

Thin Film Standardless Standardless Quantitative Analysis
Fitting Coefficient : 0.9559

Element	(keV)	Mass%	Counts	Sigma	Atom%	Compound	Mass%	Cation	K
H K									
C K	0.277	17.42	326407.28	0.03	66.89				1.1522
S K	2.307	4.45	314464.25	0.02	6.41				0.3059
Ag L (Ref.)	2.984	43.43	937777.94	0.08	18.57				1.0000
Au M	2.120	34.70	720079.94	0.08	8.13				1.0407
Total		100.00			100.00				

Fig. S15 Spot EDS spectrum of the reacted particle (Fig. 4B). Elemental composition was quantified for the presence of Sulfur (S), Silver (Ag), and Gold (Au) present in the layer-by-layer planar assembly.

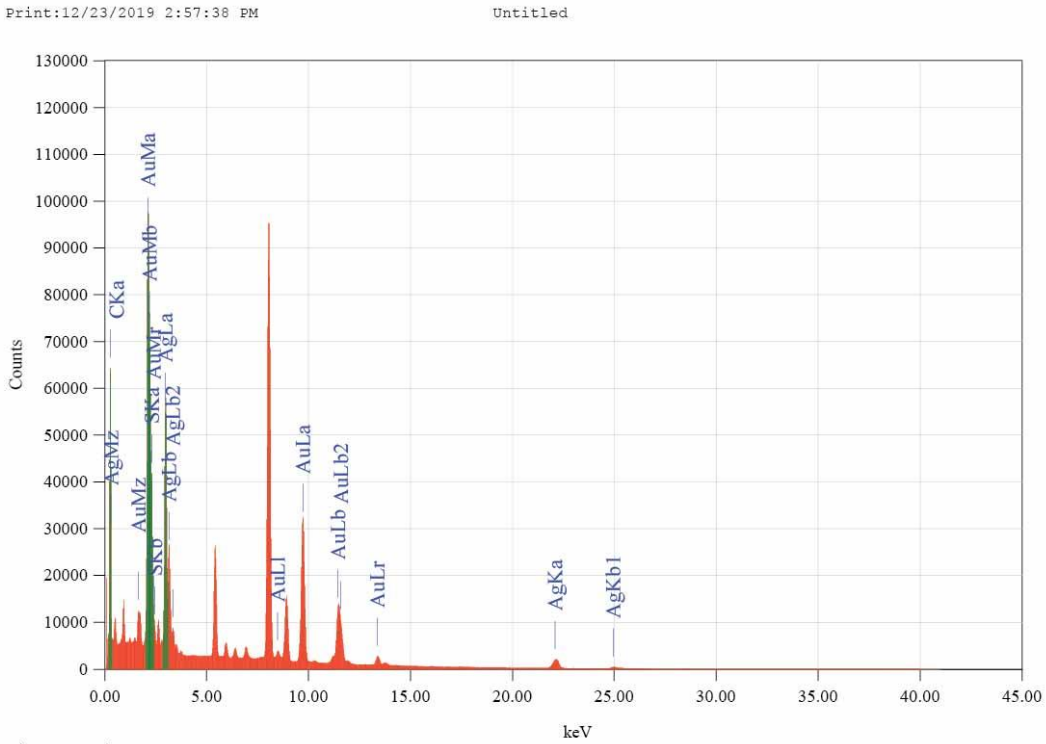

File: Untitled
Specimen ID:
Date: 12/23/2019 2:30:33 PM

Acquisition Parameter

Acc. Voltage	: 200.0 kV	Probe Current	: 1.00000 nA
Real Time	: 672.69 sec	Dead Time	: 22 %
Live Time	: 524.22 sec	Counting Rate	: 23270 Counts/sec
Preset	: Off		
Energy Range	: 0 - 40 keV	PHA Mode	: T3

Thin Film Standardless Standardless Quantitative Analysis
Fitting Coefficient : 0.5976

Element	(keV)	Mass%	Counts	Sigma	Atom%	Compound	Mass%	Cation	K
H *									
C K	0.277	19.29	403043.19	0.03	70.70				1.1072
S K	2.307	4.53	356276.50	0.02	6.21				0.2939
Ag L	2.984	32.83	790207.94	0.06	13.40				0.9609
Au M (Ref.)	2.120	43.36	1002878.75	0.08	9.69				1.0000
Total		100.00			100.00				

Fig. S16 Spot EDS spectrum of the reacted particle (Fig. 4C). Elemental composition was quantified for the presence of Sulfur (S), Silver (Ag), and Gold (Au) present in the disc-shaped assembly.

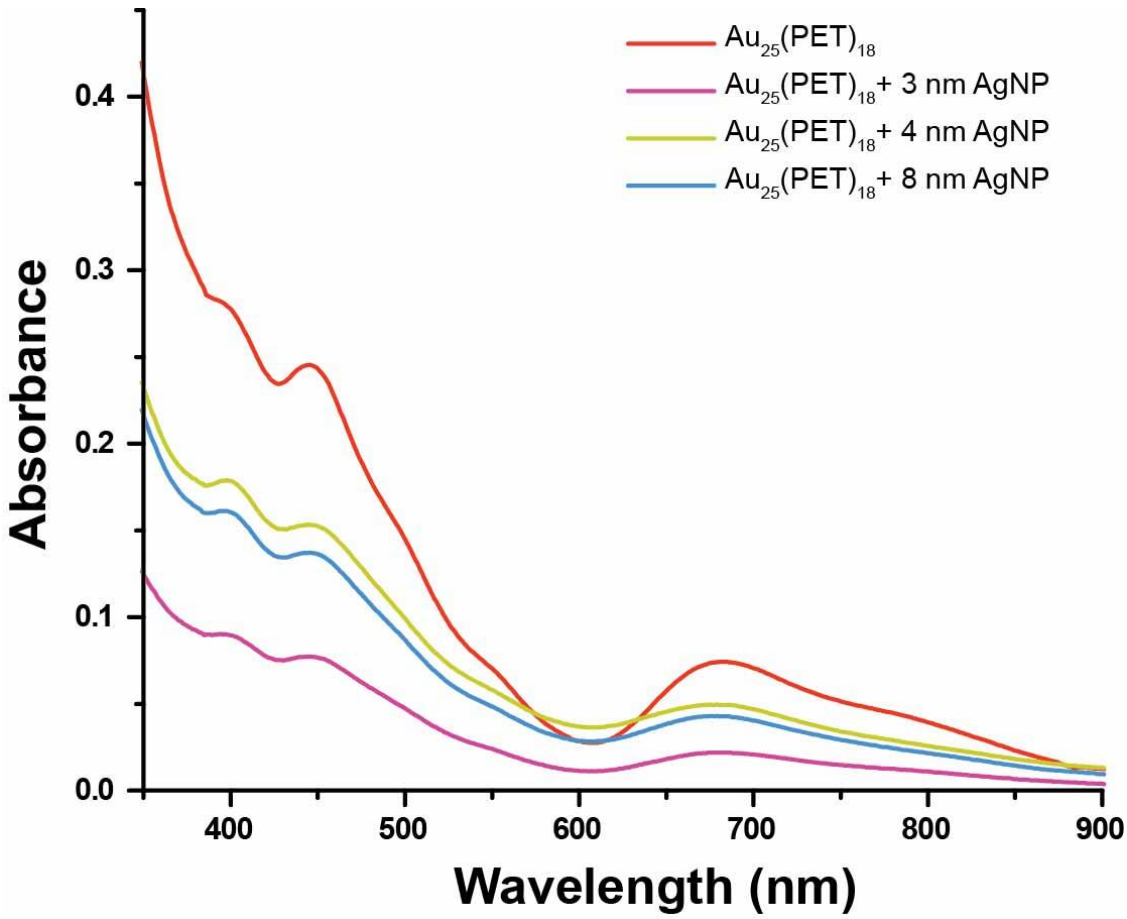

Fig. S17 The reaction mixture was monitored at the 2 min interval using UV-Vis spectroscopy, in ESI MS experimental condition (Fig. 4), for differently sized Ag@PET NPs, polydispersed 8 (blue trace, Fig. 4 B), 4 (yellow trace, Fig. 4 C), 3 nm (magenta trace, Fig. 4 D), and the parent NC (red trace, Fig. 4 A). The shifts are present in all the cases that confirms the generation of new species in all the three case at the particular time.

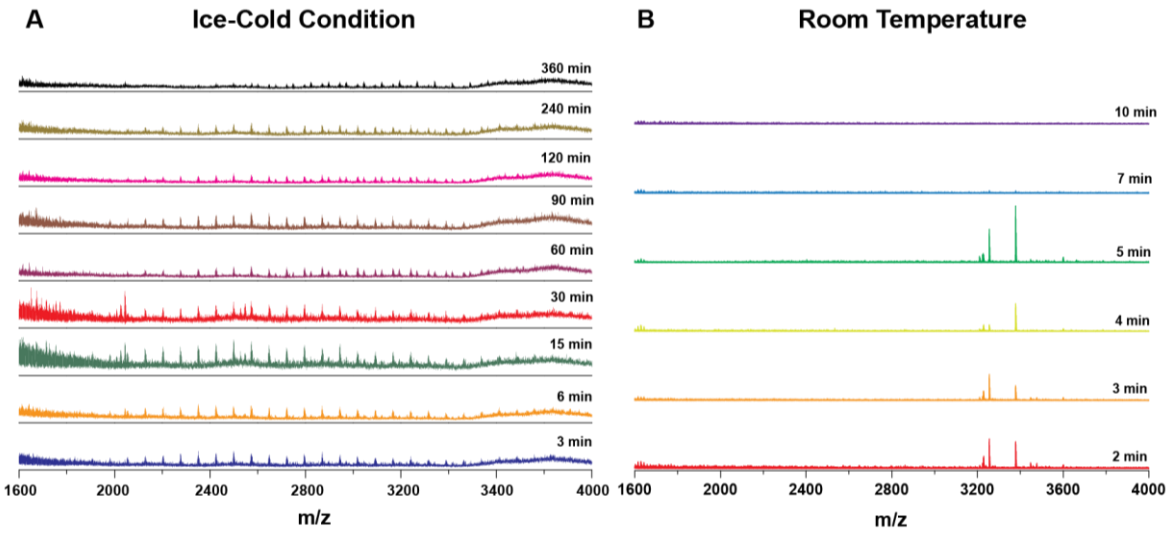

Fig. S18 Time dependent low temperature reaction monitoring of 4 nm Ag@PET NPs with $Au_{25}(PET)_{18}$ at two temperatures, namely ice-cold condition and room temperature. (A) Reaction mixture was analysed in ESI MS at ice-cold condition for 3, 6, 15, 30, 60, 90, 120, 240 and 360 min. (B) The reaction was monitored at room temperature. Spectral region of m/z 1600-4000 is plotted to compare evolution of the thiolate intermediates under two different conditions.

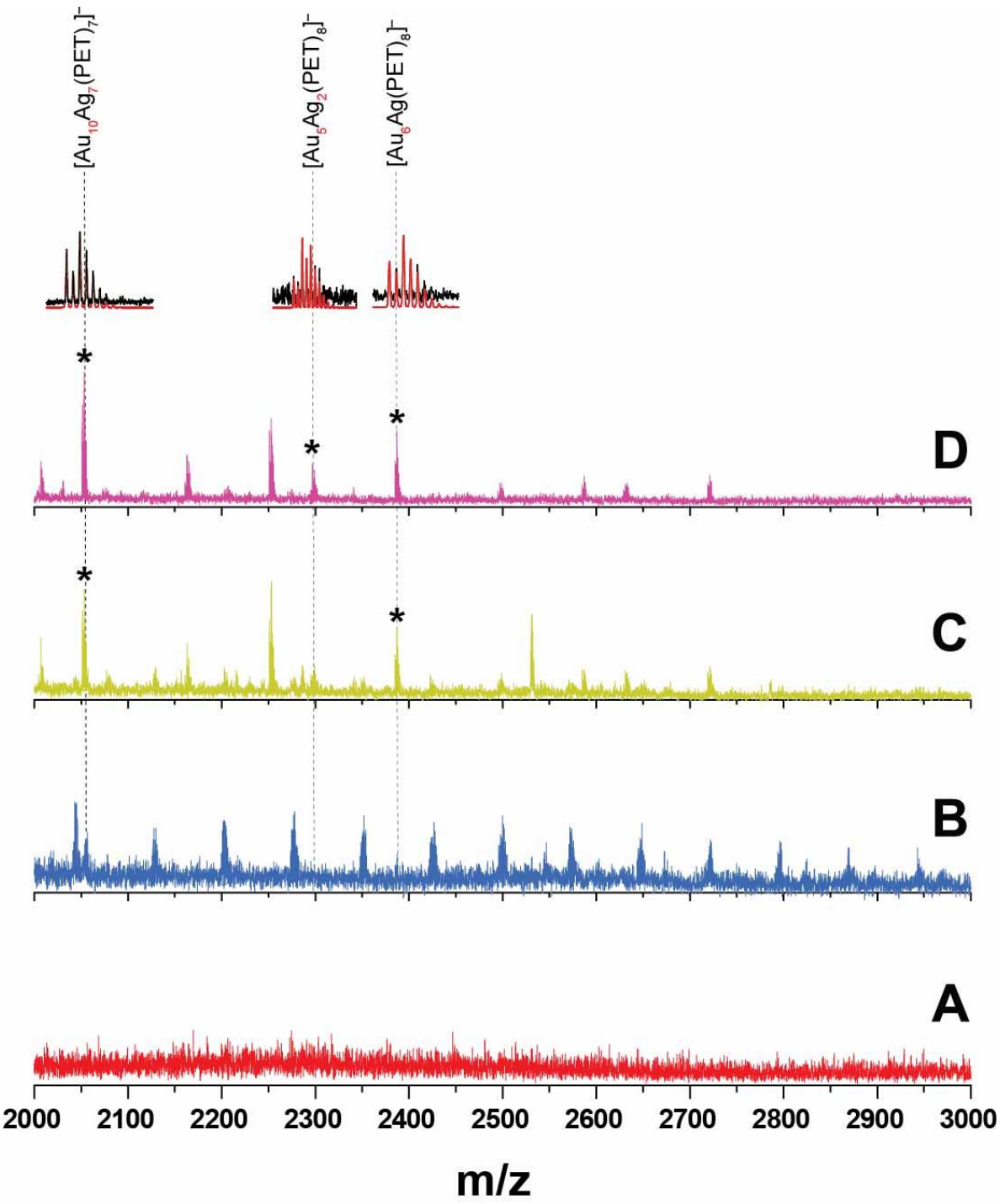

Fig. S19 Size dependent reactivity monitored using ESI MS (Fig. 4), expanded region m/z 2000-3000. The reaction fragments were found to vary for Ag@PET NPs for different sizes, (B) polydispersed 8 nm, (B) 4 nm, and (D) 3 nm. The exchange was compared with the (A) parent $Au_{25}(PET)_{18}$ cluster. Each spectrum is normalised w.r.t its corresponding $Au_{25}(PET)_{18}$ peak intensity for visual comparison.

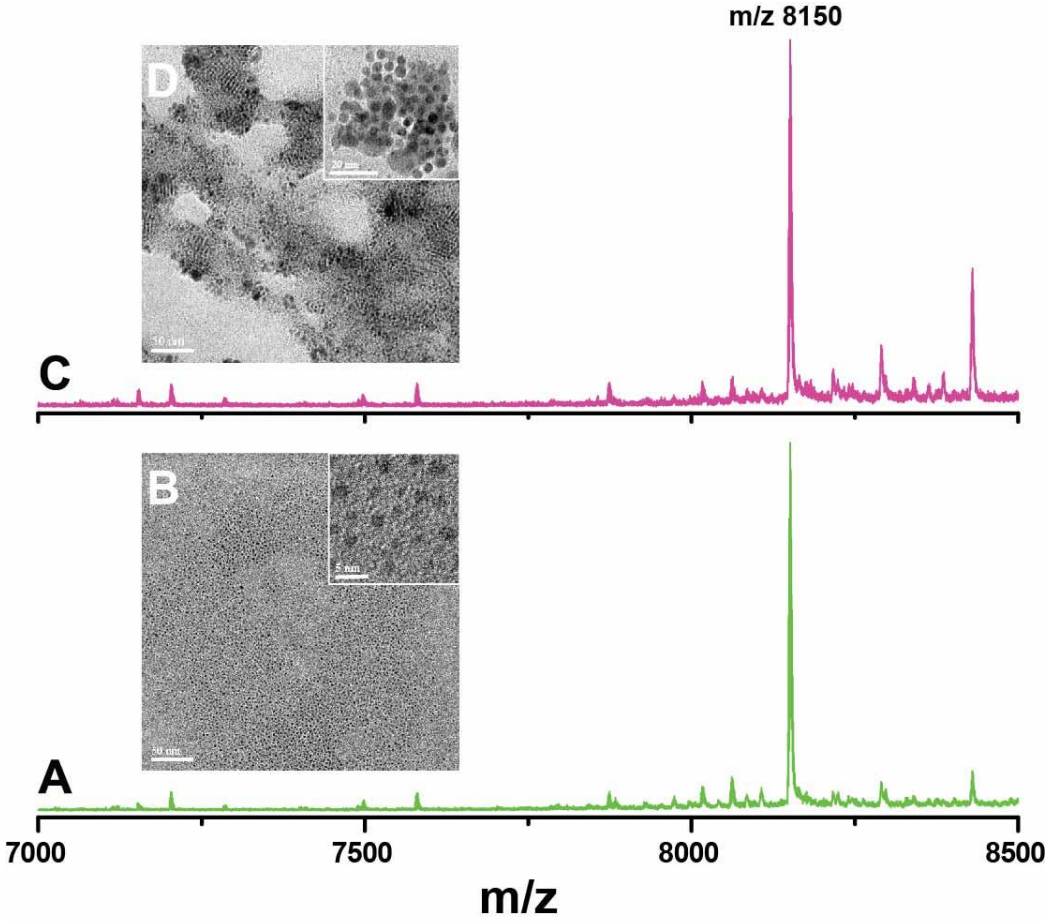

Fig. S20 Ligand specificity in the discussed reaction was explored on reacting 4 nm Ag@PET NPs with $Au_{25}(SBB)_{18}$ NC. The pure $Au_{25}(SBB)_{18}$ NC was characterized using (A) ESI MS, molecular peak at m/z 8150, and (B) HRTEM micrographs, at 50 nm and 5 nm (inset) magnifications. The reaction mixture was analysed after 2 min using (C) ESI MS, showed absence of new peaks, (D) HRTEM micrograph, no new morphology was observed unlike the previous cases (Fig. 1, 3). All the spectra were plotted to its original intensities.

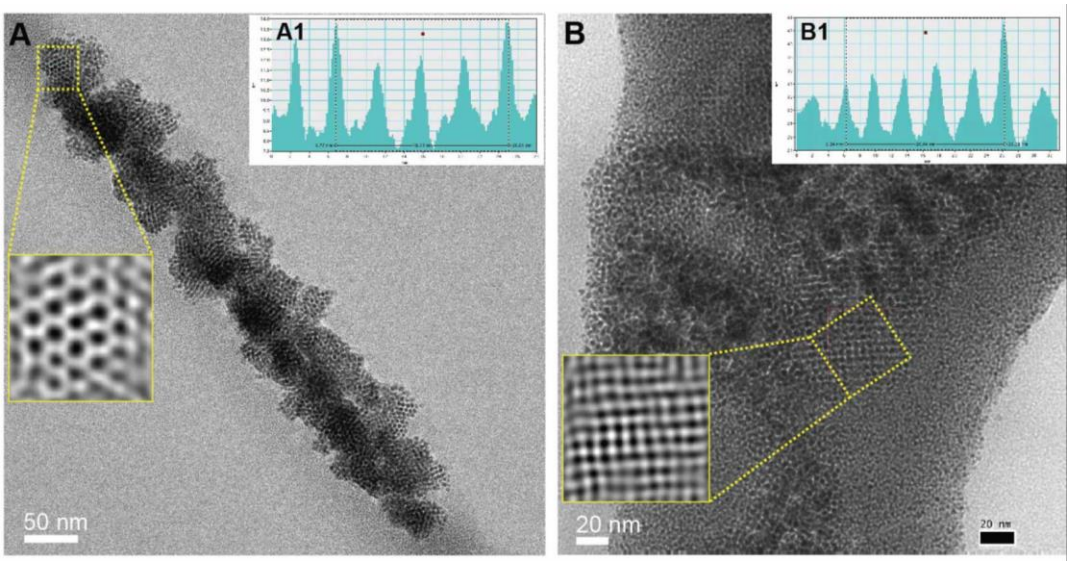

Fig. S21 Inverse fast Fourier transform (IFFT) for (A) superlattice of the reacted 4 nm Ag@PET NP, (A1) profile, and (B) layer-by-layer of the reacted 8 nm Ag@PET NP, (B1) profile.

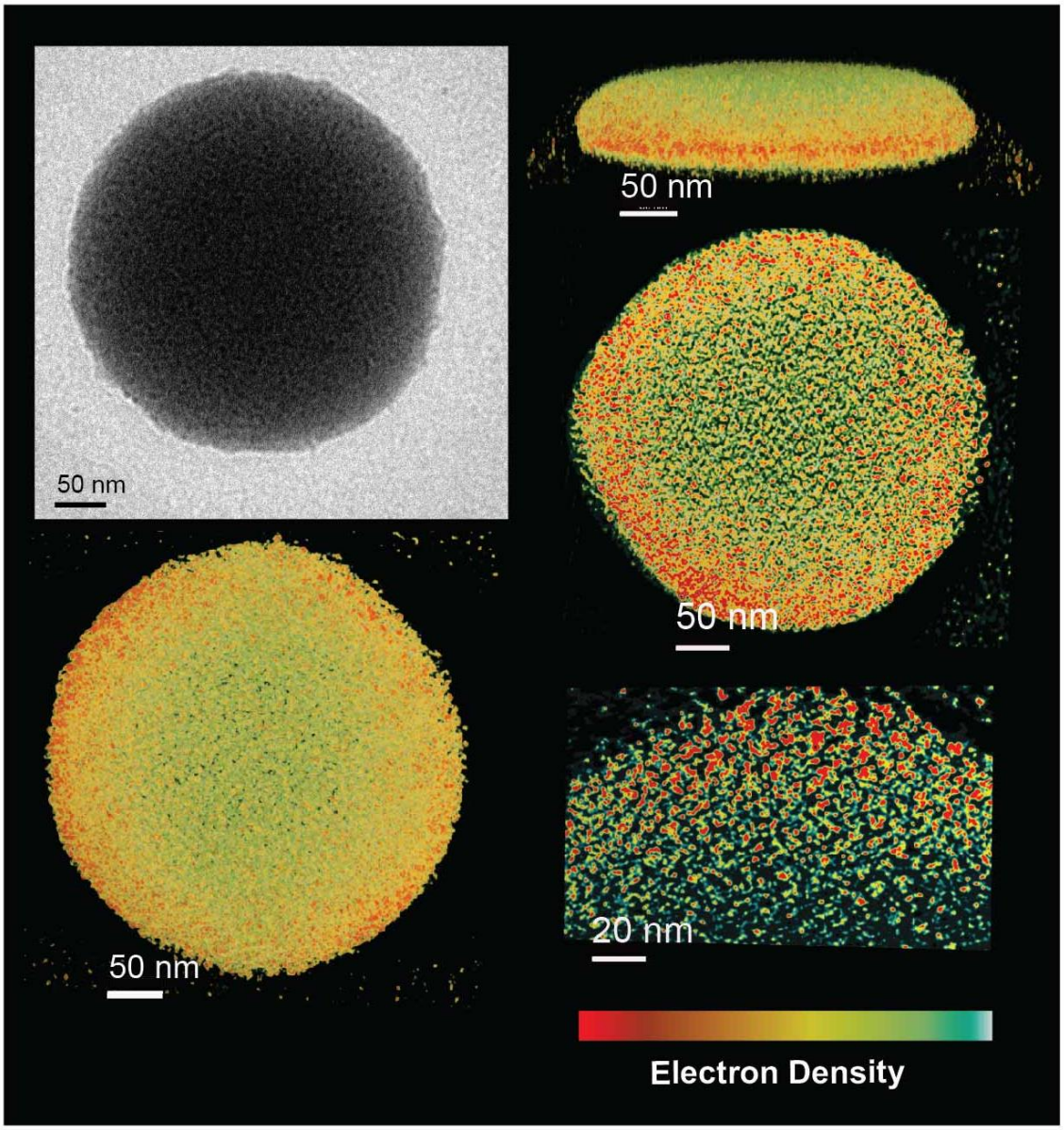

Fig. S22 Electron Tomography and 3D reconstruction a disc-shaped assembly: 2D projection followed by its corresponding 3D reconstruction for the reacted 8 nm Ag@PET NPs assembled as disc densely filled with particles. The tilt series and 3D reconstruction for the assembly is provided as Video V5, and Video V6, respectively.

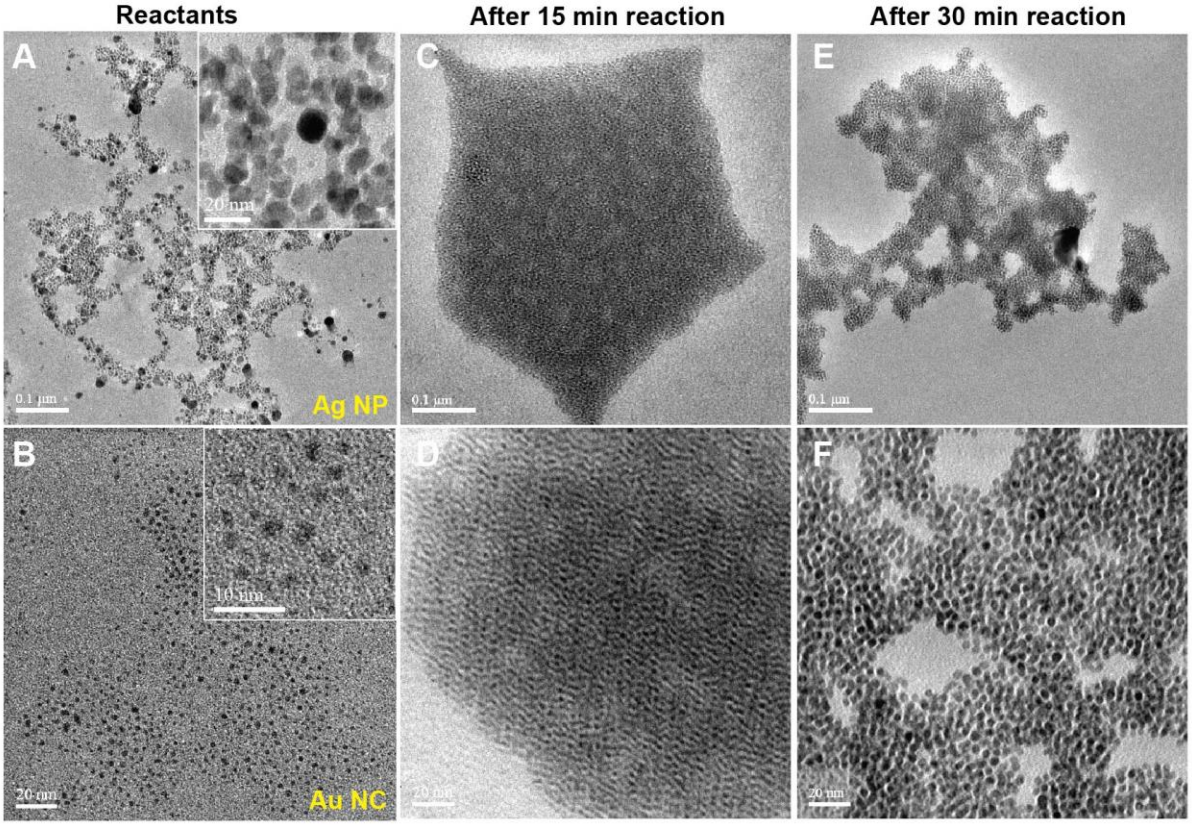

Fig. S23 HRTEM micrographs of the reaction progress for a reaction between parent 8 nm Ag@PET NP (A), and $Au_{25}(PET)_{18}$ NC (B). The products of the reaction after 15 (C, D) and 30 (E, F) min of reaction are also shown.

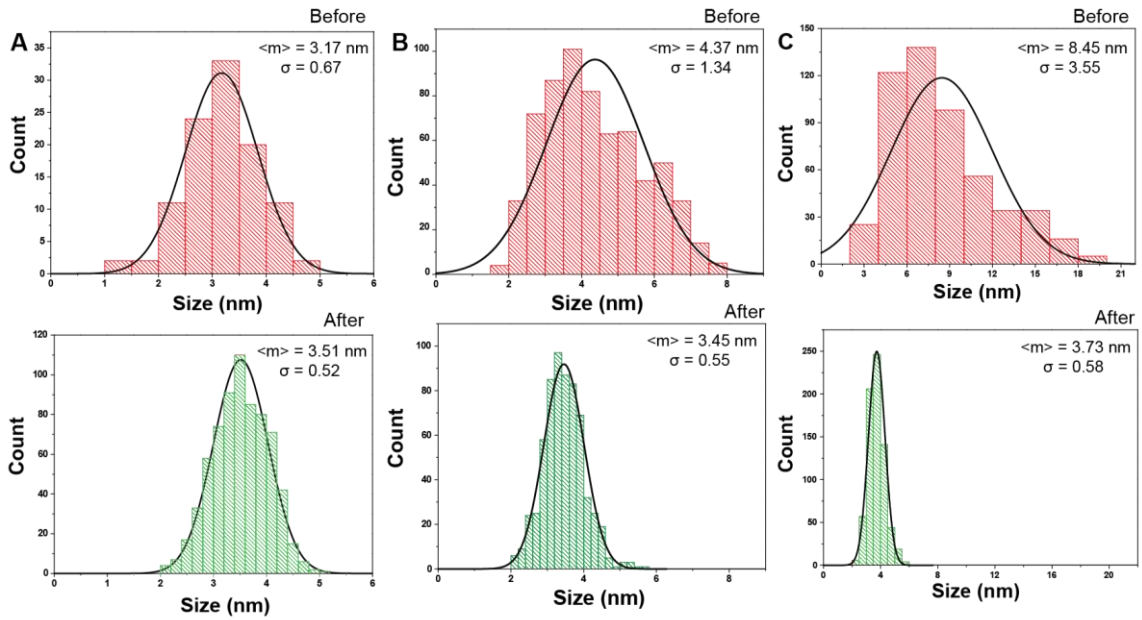

Fig. S24 Effect of NP-NC reaction on the particle size distribution. Before and after reaction with Ag NPs with average size of (A) 3, (B) 4 and (C) 8 nm, where <m> and σ are the notations used for mean size and standard deviation, respectively.

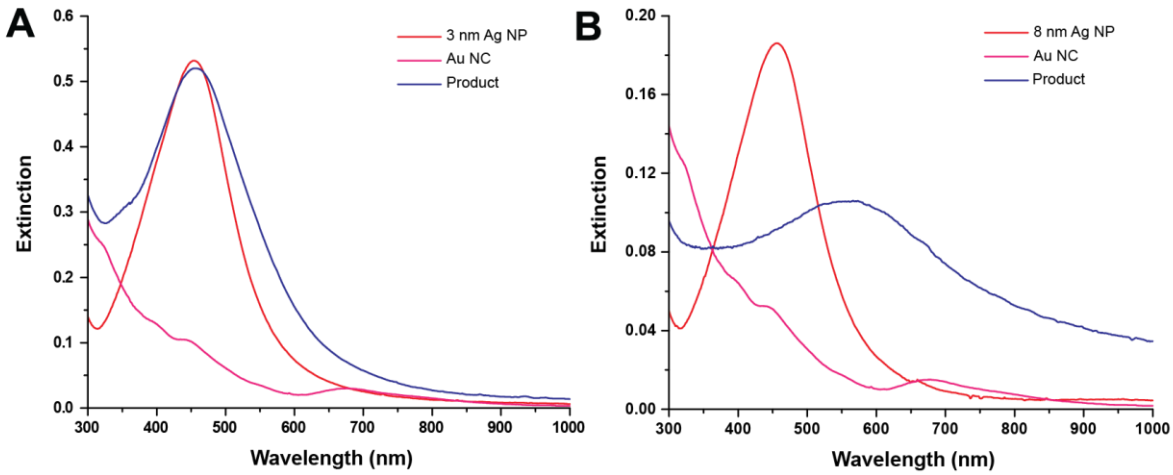

Fig. S25 UV-Vis spectra of NP-NC reaction for (A) 3 and 8 nm Ag@PET NPs. Spectra are due to Ag NP (red trace), $Au_{25}(PET)_{18}$ NC (magenta trace), and the reaction product (blue trace). The broadening of the peak upon reaction is in agreement with the gradual formation of an assembly of the reacted NPs. Also see HRTEM micrographs of the reaction products for 3 and 8 nm Ag NPs in Fig. 3B and D.

REFERENCES

1 D. N. Mastronarde, *J. Struct. Biol.*, 2005, **152**, 36–51.

2 D. N. Mastronarde, *Microsc. Microanal.*, 2003, **9**, 1182–1183.

3 N. Nonappa and P. Engelhardt, *Imaging Microsc.*, 2019, **21**, 22–24.

4 J. R. Kremer, D. N. Mastronarde and J. R. McIntosh, *J. Struct. Biol.*, 1996, **116**, 71–76.

5 P. Engelhardt, in *Electron Microscopy: Methods and Protocols*, ed. J. Kuo, Humana Press, Totowa, NJ, 2007, pp. 365–385.

6 P. Engelhardt, *Electron Tomography of Chromosome Structure*, 2006.

7 K. R. Krishnadas, A. Ghosh, A. Baksi, I. Chakraborty, G. Natarajan and T. Pradeep, *J. Am. Chem. Soc.*, 2016, **138**, 140–148.

8 A. Baksi, P. Chakraborty, A. Nag, D. Ghosh, S. Bhat and T. Pradeep, *Anal. Chem.*, 2018, **90**, 11351–11357.